Divalent counterion-induced condensation of triple-strand DNA

Xiangyun Qiu[a,1], V. Adrian Parsegian[b], and Donald C. Rau[c]

[a]Department of Physics, George Washington University, Washington, DC 20052; [b]Department of Physics, University of Massachusetts, Amherst, MA 01003; and [c]Laboratory of Physical and Structural Biology, Program in Physical Biology, National Institutes of Health, Bethesda, MD 20892

Edited by Robert Baldwin, Stanford University, Stanford, CA, and approved October 26, 2010 (received for review March 22, 2010)

Understanding and manipulation of the forces assembling DNA/RNA helices have broad implications for biology, medicine, and physics. One subject of significance is the attractive force between dsDNA mediated by polycations of valence ≥3. Despite extensive studies, the physical origin of the "like-charge attraction" remains unsettled among competing theories. Here we show that triple-strand DNA (tsDNA), a more highly charged helix than dsDNA, is precipitated by alkaline-earth divalent cations that are unable to condense dsDNA. We further show that our observation is general by examining several cations (Mg^{2+}, Ba^{2+}, and Ca^{2+}) and two distinct tsDNA constructs. Cation-condensed tsDNA forms ordered hexagonal arrays that redissolve upon adding monovalent salts. Forces between tsDNA helices, measured by osmotic stress, follow the form of hydration forces observed with condensed dsDNA. Probing a well-defined system of point-like cations and tsDNAs with more evenly spaced helical charges, the counterintuitive observation that the more highly charged tsDNA (vs. dsDNA) is condensed by cations of lower valence provides new insights into theories of polyelectrolytes and the biological and pathological roles of tsDNA. Cations and tsDNAs also hold promise as a model system for future studies of DNA–DNA interactions and electrostatic interactions in general.

DNA condensation | small angle X-ray diffraction

Highly charged DNA helices naturally repel each other under physiological conditions (1). However, cations of valence ≥3 very effectively condense DNA at micromolar concentrations (2). The most studied systems are the condensation of dsDNA with cobalt^{3+} hexammine and the biogenic polyamines (spermidine^{3+} and spermine^{4+}), whereas polymer-based cations are being exploited as DNA packaging agents for gene delivery (3). In contrast, nonspecifically interacting monovalent and divalent cations [i.e., excluding base-coordinating transition-metal ions (4) such as Mn^{2+}, Ni^{2+}, and Cu^{2+}], even at *molar* concentrations, do not condense dsDNA from dilute solution (2). The prominent role of cation valence has promoted electrostatic interaction as the primary candidate to explain this multivalent cation mediated DNA–DNA attraction (1). Whereas it is clear that further considerations must be made beyond the mean field Poisson–Boltzmann (PB) treatment, which always predicts like-charge repulsion, the physical basis for DNA condensation is still under intensive debate (5).

The multifaceted nature of DNA–ion interactions and of possible DNA–ion–DNA correlations between apposing helices has led to theories that differ greatly in starting assumptions. For instance, counterions have been treated either as continuous ionic "clouds" or as discrete point-like cations of finite radius; the DNA helix has been modeled as a continuously charged rod or to have discretely charged phosphates placed on a helical path around a smooth rod. As a result, a number of competing theories have been proposed to explain cation mediated DNA–DNA attraction. Counterion-centered mechanisms include ion density fluctuations (6), ion–ion correlations (7) possibly leading to "Wigner-crystal" ionic ordering (8, 9), strong electrostatic coupling (10), and the restructuring of DNA hydration shell by ions (11). When a discretely charged DNA is considered, cations may be significantly localized by *local* molecular electrostatic fields. Multivalent cations can transiently invert the local charge and create net attraction (12–15). Modern sophisticated theories have explicitly considered the size of cations and the effect of coions to explain a wide range of observations (16, 17). Numerical simulations have been able to reproduce multivalent counterion-induced inter-DNA attraction in silico (18), but unable to assess the underlying mechanisms due to varying levels of simplifications of the polyelectrolyte solutions (19).

Critical evaluations of existing theories are further complicated by the physical "nonideality" of the experimental systems. One issue is the real nature of the commonly used condensing ions: Cobalt hexammine is a coordination metal complex; spermidine and spermine are chain-like molecules with distributed monocharges. Treating counterions as charged spheres can be flawed (20), though commonly practiced. Furthermore, the grooves of dsDNA can be binding sites for cations, and the exposed polar groups may even coordinate specific counterions (4). Such structure-specific interactions (i.e., cations residing in the grooves) would strongly favor the proposed "zipper mechanism" for DNA–DNA attraction (21).

We have investigated the system of simple point-like cations (e.g., Mg^{2+}) and triple-strand DNA (tsDNA). Starting with a dsDNA, a tsDNA is formed by a third strand binding into the dsDNA major groove via Hoogsteen base pairing (22). Helical parameters of tsDNA (23) deviate from that of conventional B-form DNA (B-DNA): The number of base triads per turn is 12 (vs. 10.5 for B-DNA); diameter is ∼22.5 Å (∼20 Å for B-DNA). The phosphate groups of tsDNA's constituent three strands face out and are more evenly spaced, giving tsDNA a "smoother" surface and ∼40% higher charge density than dsDNA. With its bases more extensively hydrogen bonded and buried inside, tsDNA grooves are much less accessible than dsDNA for specific cation binding (23). For these reasons, DNA triplex is a promising model system to study the physics of DNA condensation.

Triple-strand DNA is also relevant to biology and pathology (24). Discovered in the 1950s, tsDNA is now known to participate in diverse biological functions such as gene regulation and DNA repair (25). Moreover, formation of tsDNA has been conjectured to underlie trinucleotide–repeat–expansion-related genetic diseases (26). Key to its biological specificity, the stability of tsDNA strongly depends on the sequence. A homopurine (R)–homopyrimidine (Y) dsDNA is usually required as the "substrate," whereas the third strand can be the same Y or the mirror repeat

Author contributions: X.Q., V.A.P., and D.C.R. designed research; X.Q. and D.C.R. performed research; X.Q. and D.C.R. contributed new reagents/analytic tools; X.Q., V.A.P., and D.C.R. analyzed data; and X.Q., V.A.P., and D.C.R. wrote the paper.

The authors declare no conflict of interest.

This article is a PNAS Direct Submission.

Freely available online through the PNAS open access option.

[1]To whom correspondence should be addressed. E-mail: xqiu@gwu.edu.

This article contains supporting information online at www.pnas.org/lookup/suppl/doi:10.1073/pnas.1003374107/-/DCSupplemental.

of the R, giving rise to either a RY*R or RY*Y tsDNA. DNA triplexes of arbitrary sequences can be stabilized with modified nucleotides (27) and have been exploited for targeting specific genes of interest (24).

Results

Our first and surprising observation is that "simple" alkaline-earth divalent cations, unable to condense dsDNA, can condense tsDNA at millimolar concentrations. The poly(AT*T) triplex is soluble in 5 mM $MgCl_2$ 1×TE (10 mM pH 7.5 Tris, 1 mM EDTA) buffer. However, an increase of [$MgCl_2$] to 10 mM leads to instant clouding and precipitation, in drastic contrast to the solubility of dsDNA in $MgCl_2$ as high as 2 M. This observation is significant as all previous reports of tsDNA condensation were with multivalent (≥3) counterions (28, 29) that also condense dsDNA.

In consideration of the homopolymeric nature of the poly (AT*T) tsDNA, we have taken careful steps to rule out intertriplex cross-linking (i.e., the third strand spanning two separate double strands) as a possible cause for condensation (see *SI Appendix* for details). Briefly, samples were annealed at low DNA concentrations of ~30 μg/mL (referred to as "as-annealed" triplex hereafter) to effectively remove intertriplex cross-linking in the stock. The other likely complication is the presence of single- or double-strand overhangs near the ends. We therefore treated the poly(AT*T) triplex with either nuclease S1 (to digest single-strand DNA) or DNase I (to digest single- and double-strand DNA). Like the as-annealed (i.e., undigested) triplex, both digested triplexes precipitate promptly in 10 mM $MgCl_2$ 1×TE solution. Triplex condensation is also fully reversible: The poly (AT*T) pellet dissolves in a few seconds when transferred to 1 mM $MgCl_2$ 1×TE buffer, and adjusting [Mg^{2+}] back to 10 mM precipitates it again. The pellets before and after this cycling process give identical X-ray diffraction peaks (discussed later). Divalent cation Mg^{2+} thus appears to induce *intertriplex attraction* that condenses the poly(AT*T) tsDNA.

We next determined whether the observed tsDNA condensation is specific to poly(AT*T) or Mg^{2+}, particularly because condensation of dsDNA or tsDNA by simple *divalent* cations such as Mg^{2+} has not been observed in free solution except in 2D (30). We first examined several divalent cations that are generally considered to interact nonspecifically with DNA. We found that the point-like Ba^{2+} and Ca^{2+} ions precipitate the poly(AT*T) and that the chain-like Putrescine^{2+} does not. Furthermore, we examined a second tsDNA helix constructed from three 21-base oligonucleotides, the RY*R-21 triplex. The same behavior was observed, i.e., precipitation by Mg^{2+}, Ba^{2+}, and Ca^{2+}, but not by Putrescine^{2+}. We emphasize that the two constructs are significantly different: Poly(AT*T) is a much longer (~300 bases), homopolymeric, RY*Y triplex, whereas the RY*R-21 is a 21-base long, mixed-sequence, RY*R triplex. Therefore, tsDNA condensation by simple alkaline-earth divalent cations proves to be general.

We proceeded to characterize the condensed tsDNA phase. The triplex pellets show optical birefringence under polarized light and give sharp X-ray diffraction peaks that can be indexed as a two-dimensional hexagonal lattice (Fig. 1*A*). The condensed tsDNA is thereby an ordered liquid crystal as observed with multivalent-cation-condensed dsDNA. Such a well-defined structure also argues against significant intertriplex cross-linking that presumably leads to unstructured gel-like aggregates. It is worth emphasizing that the same diffraction peak profiles (i.e., position and width) are obtained from the as-annealed, nuclease S1 digested, and DNase I digested poly(AT*T) triplexes (Fig. 1*B*). In 50 mM $MgCl_2$ at 20 °C, the poly(AT*T) and RY*R-21 triplexes show the same interaxial spacing of 29.8 Å, which weakly depends on [$MgCl_2$] up to 2 M. Triplexes condensed by Ca^{2+} and Ba^{2+} also give well-defined diffraction peaks (Fig. 1 *C* and *D*) and show cation-dependent interaxial spacings in the order Ba^{2+} > Mg^{2+} > Ca^{2+} [30.2, 29.8, and 29.6 Å, respectively, for poly(AT*T) triplex]. Note that the same order of spacings was observed in (Ba^{2+}, Mg^{2+}, Ca^{2+})-dsDNA complexes condensed by external osmotic stress (31). For direct comparison between dsDNA and tsDNA, we used spermine^{4+} as the common condensing ion (32). In 2 mM spermine at 20 °C, 30.0 and 28.7 Å interaxial spacings were observed for the poly(AT*T) triplex and poly(AT) duplex,

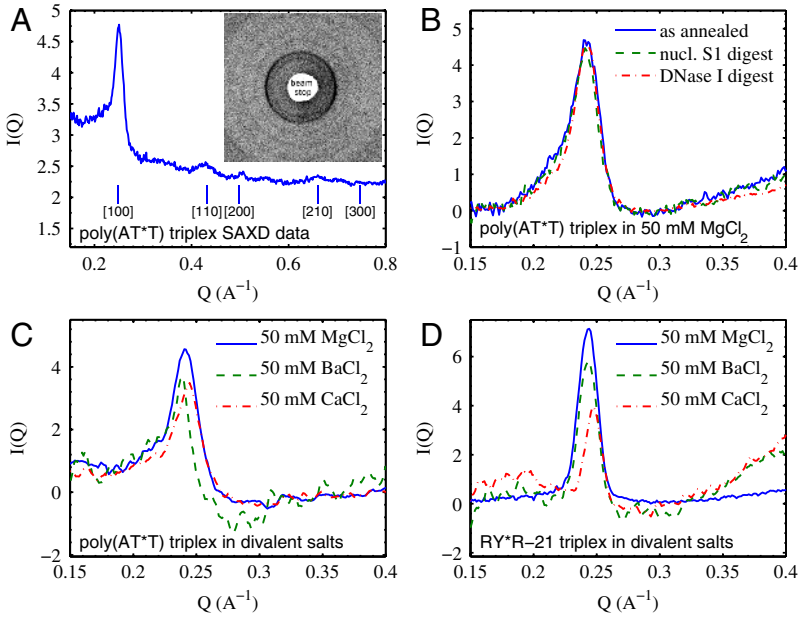

Fig. 1. Small angle x-ray diffraction (SAXD) profiles of the poly(AT*T) and RY*R-21 triplexes. I(Q) is the scattering intensity, with $Q = \frac{4\pi}{\lambda}\sin\theta$, where 2θ is the scattering angle and λ is the X-ray wavelength. Note that a linear background has been subtracted to show the peaks in *B*–*D*. (*A*) Typical raw image and the integrated profile of condensed poly(AT*T) arrays. Some higher-order peaks can be identified as weak rings, and they can be indexed with a 2D hexagonal lattice. (*B*) SAXD peak profiles of as-annealed, nuclease S1 digested, and DNase I digested poly(AT*T) tsDNA. (*C*) SAXD peak profiles of poly(AT*T) triplexes condensed by divalent cations Mg^{2+}, Ba^{2+}, and Ca^{2+} corresponding to interaxial spacing of 29.8, 30.2, and 29.6 Å, respectively. (*D*) SAXD profiles of RY*R-21 triplexes condensed by divalent cations Mg^{2+}, Ba^{2+}, and Ca^{2+} corresponding to interaxial spacing of 29.8, 30.1, and 29.3 Å respectively.

respectively; 29.8 and 28.4 Å were observed for the RY*R-21 triplex and RY-21 duplex, respectively (Fig. 2), noting that spermine-condensed high molecular weight chicken blood dsDNA (CB-dsDNA) gives an interaxial spacing of 28.3 Å. Considering the ~2.5 Å difference in helical diameters, spermine-condensed tsDNA thus has a smaller surface separation (by ~1.2 Å) than condensed dsDNA, suggesting spermine mediates stronger attraction between tsDNA than between dsDNA.

Similar to multivalent-cation-condensed dsDNA (11), tsDNA helices condensed by Mg^{2+} remain highly hydrated, e.g., ~7.3 Å solvent layer between tsDNA surfaces. To probe the extent of water structuring of this solvent layer, we examined the temperature dependence of the interaxial spacing (i.e., the thickness of the solvent layer). Fig. 3 shows that the interaxial spacing decreases upon increasing temperature for both poly(AT*T) and RY*R-21 triplexes. Although such heat-induced "collapse" is reminiscent of hydrophobic interactions, the observation with DNA is of hydrophilic and electrostatic nature and will be discussed below. Again, thermal contraction argues against the occurrence of intertriplex cross-linking, which is expected to weaken (i.e., increasing interaxial spacing) upon heating.

The finite nonzero equilibrium spacing between apposing helices indicates a balancing point between attractive and repulsive DNA–DNA forces. The net force (or repulsion) at closer DNA–DNA spacings can be measured using the osmotic stress technique coupled with X-ray scattering (33). We first verified that stressing the DNA phase (i.e., pushing DNA helices closer with osmotic stress) is a fully reversible process, i.e., cycling back and forth between unstressed and stressed tsDNA strands does not change their respective interaxial spacings. Fig. 4 shows the pressure-spacing curves of tsDNA together with the curves from multivalent-cation-condensed CB-dsDNA that have been extensively characterized previously (11). The parallel force curves from tsDNA and dsDNA condensed by different cations suggest a common physical origin for DNA–DNA interaction.

Discussion

In summary, we observed the condensation of tsDNA, a helix with more evenly spaced charges than dsDNA, by point-like divalent cations in free solution. This well-defined experimental system differs from other often-studied polyelectrolytes (such as F-actin and fd virus with charged patches of both signs) and other condensing polycations with complex structure (such as cobalt^{3+} hexammine and polyamines). It is nonetheless intriguing why *divalent* cation-induced tsDNA condensation was not observed before. We attribute this to the use of dilute divalent salts (<20 mM) for prevalent spectroscopic studies in the literature (22, 34), together with usually high levels of monovalent salt (~100 mM). The reason is that the threshold concentration of divalent cation for tsDNA condensation is sensitive to the level of monovalent background. When monovalent salt is reduced to nearly zero by dissolving condensed tsDNA pellets in pure divalent salts, the lowest [$MgCl_2$] to hold up the tsDNA pellet

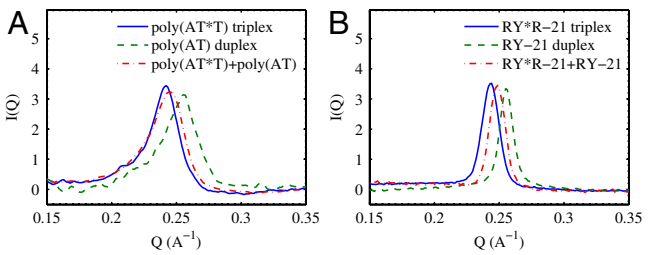

Fig. 2. Comparison of tsDNA and dsDNA condensed by 2 mM spermine^{4+}. (*A*) Poly(AT*T) triplex vs. poly(AT) duplex. The "poly(AT*T)+poly(AT)" is a mixture of the two helices of the same weight ratio. (*B*) The RY*R-21 triplex versus RY-21 duplex. The "RY*R-21+RY-21" is a mixture of the two helices of the same weight ratio.

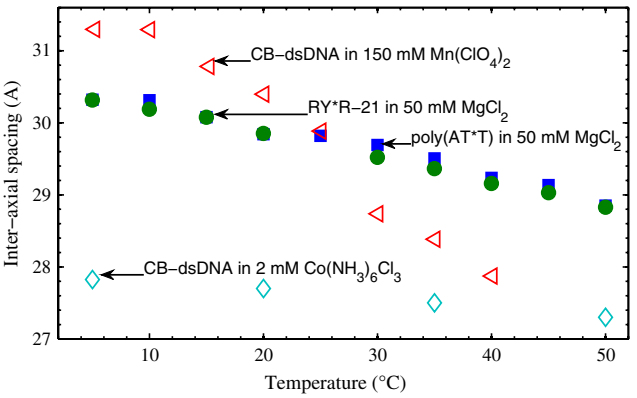

Fig. 3. Temperature dependences of the interaxial spacings of condensed tsDNA and CB-dsDNA. $Co(NH_3)_6Cl_3$ is the trivalent cobalt^{3+} hexammine chloride. Error bars for DNA interaxial spacings are around 0.1 Å and smaller than symbol sizes.

was found to be 1.5 mM. However, in 1×TE buffer, poly(AT*T) triplex is still soluble in 5 mM $MgCl_2$, whereas 10 mM $MgCl_2$ precipitates it. With the commonly used 100 mM NaCl, we found that at least 100 mM $MgCl_2$ is required to condense tsDNA; i.e., tsDNA condensation would not have occurred with the maximum 20 mM divalent salts used in the literature (22).

The specifics of our experimental system allow previously undescribed insights into the underlying physical mechanisms of counterion-mediated DNA–DNA attraction. It first appears counterintuitive that, in comparison with dsDNA, the more highly charged tsDNA is condensed by cations of lower valence (trivalent for dsDNA vs. divalent for tsDNA), whereas the opposite is expected from stronger repulsion between like-charged tsDNAs. Because the tsDNA–cation–tsDNA interaction studied here is driven by electrostatics (e.g., no specific ion coordination with DNA bases), it is suggested that tsDNA's higher propensity for condensation results from the stronger interaction between divalent cations and tsDNA charges. This is also consistent with the observation that chain-like putrescine^{2+} does not condense tsDNA, possibly because insufficient attraction is mediated due to its lower charge density than point-like ions such as Mg^{2+}. Such reasoning favors the strong DNA–cation coupling or ion–ion correlations as the origin of attraction. However, there exist a number of theories based on DNA and cation interactions (9, 10, 12–15), notably including early studies of the "Primitive Model" (6, 7). All these theories predict and rely on certain distributions of counterions along DNA helices, though unknown for both condensed dsDNA and tsDNA, to determine the DNA–DNA attraction. Knowledge of the spatial distribution of coun-

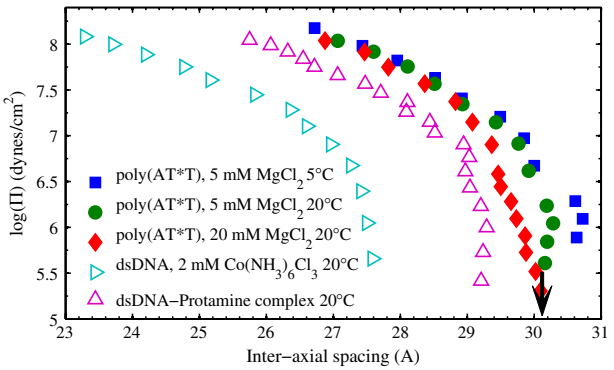

Fig. 4. The inter-DNA pressure (Π) vs. spacing curves of the poly(AT*T) triplex and CB-dsDNA. The ↓ indicates the spacing of poly(AT*T) at 20 mM $MgCl_2$ at 20 °C at zero applied pressure. Note the similarities in the distance dependence and shape in spite of different cations and DNA helices.

terions will be critical for differentiating existing theories. Nonetheless, the force measurement with osmotic stress has provided a wealth of data that are yet to be fully reproduced by existing theories of polyelectrolytes, especially noting the qualitative discrepancies over the temperature dependence discussed later.

Another interesting aspect concerns the steric role of DNA surfaces. The tsDNA grooves are less pronounced than dsDNA grooves: The minor groove of tsDNA is slightly narrower and its major groove is divided into two by the third strand. This may be significant because the grooves, if large enough, can localize cations inside and create a pattern of alternating surface charges. In particular, the "zipper" mechanism proposed for dsDNA (21) specifically considers such complementary charge correlations of adjacent dsDNA surfaces to explain DNA–DNA attraction. The grooves of tsDNA have not been observed to localize cations (23), though it is still likely for small cations such as Mg^{2+} to sit on top of tsDNA grooves coordinating two phosphates from two strands of the same tsDNA. For chain-like cations such as polyamines, their localization into the grooves is expected to depend on the dimension of grooves. We then tested whether spermine^{4+} can mediate attraction between tsDNA and dsDNA to probe the necessity of complementary DNA surfaces. Interestingly, mixed dsDNA and tsDNA helices in solution were observed to precipitate as one phase when spermine^{4+} was added, evident from the small angle X-ray diffraction (SAXD) peaks of comparable width but intermediate position (Fig. 2). Spermine^{4+} thus appears not to differentiate the two different helices with different groove patterns, arguing against the requirement of complementary surfaces for attraction. The spatial distribution of cations again is the key to understand the physical origin of attraction. Particularly for tsDNA with smoother surface, counterions may freely move within the DNA hexagonal lattice, or are arranged in fluctuating density waves, or are ordered as "Wigner" lattices. Efforts to characterize the counterion spatial distributions are under way, using Ba^{2+}-condensed tsDNA to take advantage of the high contrast of Ba^{2+} in X-ray scattering.

The close similarity of the osmotic stress force curves shown in Fig. 4 for ds- and tsDNA helices would suggest a common origin. Force measurements on dsDNA condensed by a variety of multivalent ions have extensively characterized the attractive and repulsive forces underlying DNA assembly (31). The attraction force varies exponentially with interhelical distance with an approximate 5-Å decay length (35). This force is due to the direct interaction of surfaces through either electrostatic or hydration forces. Water must necessarily restructure as the charged surfaces closely approach the last 10 Å of separation. Measured interaction energies include both that from classical charge–charge interaction through a continuum dielectric and that from water structure reorganization in close spaces. Parsing the contribution from each component is difficult. The repulsive force that prevents helices from touching is also presumed exponential with an approximate 2.5-Å decay length (36). This is an image charge repulsion within electrostatics or its hydration equivalent (31). Both electrostatics and hydration require a correlation of charges on apposing helices for attraction. For DNA surfaces with purely negatively charged groups, only repulsive hydration force is expected. However, multivalent *counterions* serve to restructure the hydration shell near the surface and create complementary water structuring and the attractive hydration force (11). The greater condensing propensity of tsDNA than dsDNA may in fact arise from its higher charge density: It is conceivable that tsDNA can "draw" counterions to a greater extent than dsDNA, and the resultant greater extent of the hydration shell restructuring leads to stronger attraction.

The consideration of water structuring also provides a consistent explanation to the temperature-induced decrease of the interaxial spacings observed in Fig. 3, as heating is expected to drive off some of the structured water near DNA surfaces. The release of structured water provides the entropic gain and leads to thermal contraction. Direct DNA–cation interactions in a continuum constant dielectric medium would have predicted thermal expansion. The magnitude of thermal contraction is not the same among different systems, in the order Co-dsDNA < Mg-tsDNA < Mn-dsDNA. The differences presumably reflect the cation-dependent restructuring of the hydration shells in the DNA–cation complex (31). We also note some other possible explanations or contributions to the observed thermal contraction. One is that temperature increase would lower the water dielectric constant, which may enhance DNA–DNA attraction and lead to closer spacing. Another possibility is that apposing DNA helices and the interstitial cations may rearrange structurally at higher temperatures for stronger attraction, though no noticeable changes in DNA packing geometry were observed in our SAXD measurements. In summary, the multifaceted nature of DNA–cation–solvent interactions proves to be a fertile ground for varied theoretical treatments, and we have yet to see one theory account quantitatively for all the experimental observations described here and in the literature. Although already providing previously undescribed insights into the physical origin of "like-charge attraction" unattainable by studying conventional dsDNA and complex cation systems alone, the well-defined physical system of tsDNA and simple cations may find good use in our future efforts to understand the electrostatic interactions of biomolecules in general.

Interestingly, both poly(AT*T) and RY*R-21 triplexes precipitate under the condition of "mimic" physiological salt: 140 mM NaCl, 10 mM $MgCl_2$, 1 mM spermine. This may have direct pathological and biological implications, as triplex-forming sequences were recently shown to exclude nucleosome assembly (37). First, tsDNA formation has been observed to correlate well with the transcription repression of frataxin and the pathogenesis (24). Our finding offers an explanation that this gene-silencing structure leading to Friedreich's ataxia, the most common inherited ataxia, can in fact be aggregated DNA triplexes effecting heterochromatin-like inhibition (38). Second, DNA triplex motifs occur frequently in eukaryotic genomes (up to 1%) (24, 39). The inter-triplex attraction under physiological conditions would significantly modulate the chromosome conformation. Moreover, the corresponding triplex motifs on homologous chromosomes can serve as "sticky alignment markers" to bring together and align the pair, facilitating homologous recombination.

Materials and Methods

Triple-Strand DNA Constructs. Both tsDNA constructs were carefully characterized to ensure their triple-strand nature (see *SI Appendix*). The first construct, poly(AT*T) tsDNA of nominal length of ~300 bases, was prepared by mixing homodeoxynucleotides poly(A) and poly(T) at 1:2 molar ratio and annealed at 94 °C in 5 mM $MgCl_2$ 1×TE (pH 7.5 10 mM Tris, 1 mM EDTA) buffer. The second construct, the 21-base RY*R-21 tsDNA, was prepared by mixing equi-molar amounts of three 21-base-long triplex forming oligonucleotides: the homopurine R strand (5′-GGAAGGAGAAGAAGGAAAGAG-3′), its complementary homopyrimidine Y strand (3′-CCTTCCTCTTCTTCCTTTCTC-5′), and its mirror repeat homopurine strand (3′-GGAAGGAGAAGAAGGAAAGAG-5′). The sequences were designed to avoid base-slip mismatches between the RY-21 duplex and the third strand. The 21-base RY*R-21 triplex and RY-21 duplex were annealed in 100 mM NaCl 10 mM $MgCl_2$ 1×TE buffer.

Chicken Blood dsDNA. Chicken blood dsDNA (CB-dsDNA) was chosen as a random-sequence dsDNA for comparison with tsDNA. Sample preparation and data collection follow ref. 11.

Experiments (*i*) Small angle X-ray diffraction. SAXD quantifies the interaxial spacings of ordered DNA arrays. Our in-house setup was described in detail in ref. 11. (*ii*) Osmotic stress method. The osmotic stress technique directly gives the force-distance relationship between DNA helices. Here the condensed

DNA phase is bathed in excess PEG solution phase under salt conditions of interest. Although PEG and DNA do not mix, small ions and water freely exchange between the two phases. DNA helices are thus "stressed" by the excluded PEG with known osmotic pressure, and the change of interaxial spacings is measured with SAXD.

ACKNOWLEDGMENTS. We thank Drs. Igor Panyutin, Victor Zhurkin, Michaela Vorlickova, Rengaswami Chandrasekaran, and Michael Seidman for helpful advice and discussions. This research was supported by the Intramural Research Program of the National Institutes of Health, Eunice Kennedy Shriver National Institute of Child Health and Human Development.

1. Gelbart WM, Bruinsma RF, Pincus PA, Parsegian VA (2000) DNA-inspired electrostatics. *Phys Today* 53:38–44.
2. Bloomfield VA (1997) DNA condensation by multivalent cations. *Biopolymers* 44:269–282.
3. Templeton NS, ed. (2008) *Gene and Cell Therapy: Therapeutic Mechanisms and Strategies* (CRC, Boca Raton, FL), 3rd Ed.
4. Hud NV, Polak M (2001) DNA-cation interactions: The major and minor grooves are flexible ionophores. *Curr Opin Struc Biol* 11:293–301.
5. Wong GCL (2006) Electrostatics of rigid polyelectrolytes. *Curr Opin Colloid Interface Sci* 11:310–315.
6. Kjellander R, Marcelja S (1984) Correlation and image charge effects in electric double-layers. *Chem Phys Lett* 112:49–53.
7. Guldbrand L, Jonsson B, Wennerstrom H, Linse P (1984) Electrical double-layer forces—A Monte-Carlo study. *J Chem Phys* 80:2221–2228.
8. Rouzina I, Bloomfield VA (1996) Macroion attraction due to electrostatic correlation between screening counterions 1. Mobile surface-adsorbed ions and diffuse ion cloud. *J Phys Chem* 100:9977–9989.
9. Shklovskii BI (1999) Wigner crystal model of counterion induced bundle formation of rodlike polyelectrolytes. *Phys Rev Lett* 82:3268–3271.
10. Naji A, Netz RR (2004) Attraction of like-charged macroions in the strong-coupling limit. *Eur Phys J E* 13:43–59.
11. Rau DC, Parsegian VA (1992) Direct measurement of the intermolecular forces between counterion-condensed DNA double helices—Evidence for long-range attractive hydration forces. *Biophys J* 61:246–259.
12. de la Cruz MO, et al. (1995) Precipitation of highly-charged polyelectrolyte solutions in the presence of multivalent salts. *J Chem Phys* 103:5781–5791.
13. Chen YG, Weeks JD (2006) Local molecular field theory for effective attractions between like charged objects in systems with strong Coulomb interactions. *Proc Natl Acad Sci USA* 103:7560–7565.
14. Tan ZJ, Chen SJ (2006) Ion-mediated nucleic acid helix-helix interactions. *Biophys J* 91:518–536.
15. Travesset A, Vaknin D (2006) Bjerrum pairing correlations at charged interfaces. *Europhys Lett* 74:181–187.
16. Solis FJ, de la Cruz MO (1999) Attractive interactions between rodlike polyelectrolytes: Polarization, crystallization, and packing. *Phys Rev E* 60:4496–4499.
17. Solis FJ, de la Cruz MO (2001) Flexible linear polyelectrolytes in multivalent salt solutions: Solubility conditions. *Eur Phys J E* 4:143–152.
18. Linse P (2000) Structure, phase stability, and thermodynamics in charged colloidal solutions. *J Chem Phys* 113:4359–4373.
19. Boroudjerdi H, et al. (2005) Statics and dynamics of strongly charged soft matter. *Phys Rep* 416:129–199.
20. Dai L, Mu YG, Nordenskiold L, van der Maarel JRC (2008) Molecular dynamics simulation of multivalent-ion mediated attraction between DNA molecules. *Phys Rev Lett* 100:118301.
21. Kornyshev AA, Leikin S (1999) Electrostatic zipper motif for DNA aggregation. *Phys Rev Lett* 82:4138–4141.
22. Soyfer VN, Potaman VN (1995) *Triple Helical Nucleic Acids* (Springer, New York).
23. Chandrasekaran R, Giacometti A, Arnott S (2000) Structure of poly (dT)-poly (dA)- poly (dT). *J Biomol Struct Dyn* 17:1011–1022.
24. Seidman MM, Glazer PM (2003) The potential for gene repair via triple helix formation. *J Clin Invest* 112:487–494.
25. Majumdar A, et al. (1998) Targeted gene knockout mediated by triple helix forming oligonucleotides. *Nat Genet* 20:212–214.
26. Wells RD (2008) DNA triplexes and Friedreich ataxia. *FASEB J* 22:1625–1634.
27. Li JS, Chen FX, Shikiya R, Marky LA, Gold B (2005) Molecular recognition via triplex formation of mixed purine/pyrimidine DNA sequences using oligoTRIPs. *J Am Chem Soc* 127:12657–12665.
28. Saminathan M, et al. (1999) Ionic and structural specificity effects of natural and synthetic polyamines on the aggregation and resolubilization of single-, double-, and triple-stranded DNA. *Biochemistry* 38:3821–3830.
29. Goobes R, Cohen O, Minsky A (2002) Unique condensation patterns of triplex DNA: Physical aspects and physiological implications. *Nucleic Acids Res* 30:2154–2161.
30. Koltover I, Wagner K, Safinya CR (2000) DNA condensation in two dimensions. *Proc Natl Acad Sci USA* 97:14046–14051.
31. Leikin S, Parsegian VA, Rau DC, Rand RP (1993) Hydration forces. *Annu Rev Phys Chem* 44:369–395.
32. Raspaud E, Durand D, Livolant F (2005) Interhelical spacing in liquid crystalline spermine and spermidine-DNA precipitates. *Biophys J* 88:392–403.
33. Parsegian VA, Rand RP, Rau DC (1995) Macromolecules and water: Probing with osmotic stress. *Method Enzymol* 259:43–94.
34. Bai Y, et al. (2007) Quantitative and comprehensive decomposition of the ion atmosphere around nucleic acids. *J Am Chem Soc* 129:14981–14988.
35. Todd BA, Parsegian VA, Shirahata A, Thomas TJ, Rau DC (2008) Attractive forces between cation condensed DNA double helices. *Biophys J* 94:4775–4782.
36. Rau DC, Lee B, Parsegian VA (1984) Measurement of the repulsive force between poly-electrolyte molecules in ionic solution—Hydration forces between parallel DNA double helices. *Proc Natl Acad Sci USA* 81:2621–2625.
37. Ruan H, Wang YH (2008) Friedreich's ataxia GAATTC duplex and GAA. GAA.TTC triplex structures exclude nucleosome assembly. *J Mol Biol* 383:292–300.
38. Saveliev A, Everett C, Sharpe T, Webster Z, Festenstein R (2003) DNA triplet repeats mediate heterochromatin-protein-1-sensitive variegated gene silencing. *Nature* 422:909–913.
39. Behe MJ (1995) An overabundance of long oligopurine tracts occurs in the genome of simple and complex eukaryotes. *Nucleic Acids Res* 23:689–695.